



Adsorption of methylene blue on activated carbon fiber prepared from coconut husk: isotherm, kinetics and thermodynamics studies

Hatem A. AL-Aoh*, Rosiyah Yahya, M. Jamil Maah, M. Radzi Bin Abas

*Faculty of Science, Department of Chemistry, University of Malaya, Kuala Lumpur 50603, Malaysia
Tel. +60 176243656; email: issa_hatem2@yahoo.com*

Received 26 April 2013; Accepted 18 June 2013

ABSTRACT

The adsorption of methylene blue (MB) on activated carbon fiber (ACF) and granular activated carbon (ACG) was studied in a batch system. The effects of initial concentration, agitation time, solution pH, and temperature were examined. Adsorption isotherms were described using both the Langmuir and Freundlich models. It was found that the Langmuir model fits well with the experimental data. The pseudo-first-order, pseudo-second-order, and intra-particle diffusion models were used to examine the kinetics data. The results obtained showed that empirical kinetics data of both ACF and ACG were only well described by the second-order model. It was observed that the ACF has adsorption performance higher than that of ACG. Adsorption thermodynamics parameters were estimated and their values indicated that the adsorption of MB on ACF and ACG were endothermic and spontaneous processes. Thermodynamic results also indicate that the adsorption of MB on both adsorbents is by chemical interaction.

Keywords: Isotherm; Kinetics; Thermodynamics; Coconut husk fiber; Activated carbon fiber; Methylene blue

1. Introduction

Methylene blue (MB) is the cationic dye that is most commonly and continuously used for dyeing cotton, wool, and silk [1]. Therefore, wastewater generated from industries related to the use and synthesis of MB is always contaminated by this organic pollutant. MB is a toxic and carcinogenic material. The toxic effects that have been described in animals exposed to MB include hypothermia, hemoconcentration, acidosis, hypercapnia, hypoxia, increases in blood pressure, corneal injury, changes in respiratory frequency and amplitude, conjunctival damage, and

Heinz body formation [2]. To identify the potential carcinogenic hazard of MB to human health, the network time protocol performed for 3 months and 2 years toxicity studies at doses of 0, 5, 25, and 50 mg/kg bw/day for rats and 0, 2.5, 12.5, and 25 mg/kg bw/day for mice, which were achieved by Camp [3] and Auerbach et al. [4], respectively. They found that the MB has carcinogenic hazard to human health especially at high doses. Moreover, it was reported that MB causes tachycardia, methemoglobinemia, cyanosis, convulsions, dyspnea, irritation to the skin and gastrointestinal tract, nausea, vomiting, and diarrhea [5,6]. Consequently, it is compulsory to remove this hazardous compound from wastewater prior to its

*Corresponding author.

disposal to the environment. For this reason, numerous methods such as coagulation, chemical precipitation, membrane filtration, solvent extraction, reverse osmosis, and adsorption have been applied for the removal of MB from industrial effluents [7]. Among these methods, adsorption has been found to be superior than other methods for wastewater treatment in terms of low cost, flexibility and simplicity of design, ease of operation, and insensitivity to toxic pollutants [6,7]. Adsorption also does not lead to the formation of harmful substances [8]. Moreover, adsorption has ability to remove any pollutant at any concentration at a relatively lower cost [6,7]. Conventionally, granulated and powdered activated carbons (granular activated carbon [ACG] and PAC) are the oldest and the most commonly used adsorbents. However, the use of commercially available ACG and PAC is limited due to their higher cost [9]. This is because the raw materials used for the preparation of this activated carbon are non-renewable and relatively expensive, such as coal [10]. Moreover, it was reported that the adsorption rate of ACG is very slow [11] and separation of ACP from the fluid after use is required [12]. Thus, low-cost adsorbents have been derived from a variety of waste materials such as chitin and chitosan [13], peat [14], rice husk [15], clay [16], bottom ash and de-oiled soya [17,18], coal ash [19], crushed bricks [20], sugar beet pulp [21], tea waste [22], feathers [23–26], bottom ash [27], de-oiled soya [28], etc. Despite the low cost of the adsorbents which developed those sold wastes, their adsorption capacities are very small. Activated carbon fiber (ACF) with its large adsorption efficiency and higher external surface area than that of the ACG [29] offers an important alternative. Recently, ACFs produced from low-cost agricultural precursors, such as oil palm fiber [10], kenaf [30], and jute fiber [5], has been proposed as low-cost and effective adsorbents for removing MB from wastewater. Coconut husk fibers are available in many tropical countries including Malaysia. In the year 2001, Malaysia used around 151,000 ha of the land for coconut plantations and is expected to produce about 5,280 kg of the dry husk per hectare yearly [31]. The Food and Agricultural Organization reported that the annual production of coconut fruit in 2009 was 54.72 million metric ton, which was then converted to about 19.15 metric ton of husk fiber as the byproduct [32]. These huge amounts of coconut husk fiber are used for making traditional products such as twine, ropes, mats, brushes, and sacks [33]. So far, there has been no attempt to use activated carbon prepared from coconut husk fiber as an adsorbent for the removal of MB from aqueous solution. Consequently, the aim of this work was to investigate the adsorption

of MB on ACF prepared from coconut husk fiber. For comparison, the adsorption of the dye on commercially available ACG was also investigated. Isotherm, kinetics, and thermodynamic aspects of the adsorption of MB on ACF and ACG were investigated in a batch adsorption system. Effects of the adsorption parameters such as initial concentration, solution pH, agitation time, and temperature on the adsorption capacity of these adsorbents were also studied.

2. Materials and methods

2.1. Preparation and characterization of the adsorbent

Coconut husk fiber-based activated carbon was prepared in a horizontal tube furnace under optimized conditions established in our earlier work. The optimized parameters were: activation temperature of 800°C, 30% w/v ZnCl₂ concentration, nitrogen flow rate of 200 cm³/min, 1 h activation time, and carbonization temperature of 300°C. The ACG (CAS No. 64365-11-3) was purchased from Sigma–Aldrich (Germany). The specific surface areas (*S*_{BET}) of ACF and ACG were measured by N₂ adsorption (at 77.40 K), using a surface analyzer (Sorptomatic Thermo Finnigan 1990, USA). The t-method was used to determine the pore structure of these adsorbents. The pH at the point of zero charge (pH_{ZPC}) was determined for both ACF and ACG using the batch equilibrium method, which has been described by Theydan and Ahmed [34]. The Fourier transform infrared spectroscopy (FT-IR) (Perkin–Elmer-2000 FT-IR) measurement was applied to quantify the surface functional groups of these two activated carbons. The surface morphology of the adsorbents used in this work was examined by scanning electron microscopy (SEM) (LEO 1455 VP, England).

2.2. Adsorbate

MB (28514 FLUKA) with purity ≥95%, molecular weight 319.85, empirical formula C₁₆H₁₈ClN₃·xH₂O, and having maximum wave length at 618 nm, was supplied by Sigma–Aldrich (USA). The structural

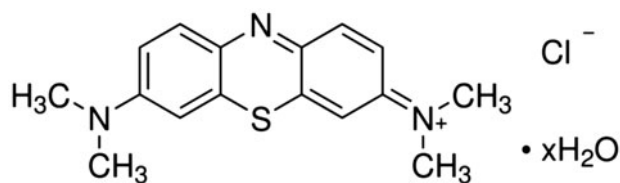


Fig. 1. The structural formula of MB.

formula is given in Fig. 1. A stock solution of 10,000 mg/L was prepared by dissolving 10 g of MB in 300 mL deionized water and diluted to 1,000 mL. The test solutions were prepared by diluting deionized water of this stock solution to the required concentrations.

2.3. Adsorption procedures

2.3.1. Effect of the adsorbate initial concentration

Experiments on the effect of the initial concentration of MB were performed in seventeen 30 mL amber bottles each containing 25 mL of MB solution at different initial concentrations (10–1,000 mg/L). Approximately, 0.03 ± 0.01 g of ACF was then added to each bottle. The bottles were mounted on a rotational shaker and shaken at 150 rpm, at room temperature ($30 \pm 1^\circ\text{C}$), and without any pH adjustment, for three days to reach equilibrium. After reaching the equilibrium, the samples were through a $0.45 \mu\text{m}$ membrane filter paper under suction. The concentrations of MB in the filtrate before and after adsorption were measured by UV–visible spectrophotometer (Shimadzu, Japan) at 618 nm. The same procedures were repeated with ACG as the adsorbent.

2.3.2. Equilibrium studies

Adsorption isotherms are helpful to explain the interaction between the adsorbent and adsorbate of any system [1]. The parameters of the isotherm models offer significant information on the adsorption mechanisms and the surface properties and efficiencies of the adsorbent [1]. However, the equilibrium data of the adsorption can be analyzed by several equations; Langmuir and Freundlich models are being the most accepted surface adsorption models in a single solute system. Therefore, only these two models were applied in this work. Experiments for the adsorption isotherms were carried out as described in Section 2.3.1.; but this time, the initial concentrations of MB used ranged from 500 to 900 mg/L.

2.3.3. Adsorption kinetics

The adsorption of 100 and 200 mg/L solutions of MB on the ACF and ACG was investigated at various time intervals. The same procedures as described in the isotherm studies were applied. The results obtained were used to investigate the effect of contact time as well as the adsorption kinetics.

2.3.4. Effect of solution pH

A series of 600 mg/L MB solutions at various initial pH (2–11) were prepared by the addition of either HCl or NaOH. Twenty-five milliliter of each of this solution was added to a 30 mL amber bottle containing 0.03 ± 0.01 g of either ACF or ACG. The bottles were then sealed, placed on a rotational shaker, and shaken for three days at 150 rpm and room temperature ($30 \pm 1^\circ\text{C}$). The adsorbent was separated from the aqueous phase by filtration through a membrane filter paper. The final concentrations of MB and adsorption amounts at equilibrium were measured and calculated.

2.3.5. Adsorption thermodynamics

The adsorptions of 500, 600, and 700 mg/L solutions of MB on these two adsorbents were studied at 30, 45 and, 60°C using an incubator shaker. The other procedures carried out were similar to those of the isotherm studies. The results obtained were used to examine the impact of temperature and to determine the adsorption thermodynamic parameters.

3. Results and discussion

3.1. Characterization of the activated carbons

The results of the surface analysis and pH_{ZPC} of the ACF and ACG are summarized in Table 1. It can be observed from this table that ACF has a larger surface area, larger total pore volume, larger mesopore volume, and higher mesopore percentage mesopore than that of ACG. This indicates that the adsorptive properties of the former are better than those of the latter.

Figs. 2 and 3 represent the SEM photograph of the prepared ACF and commercial activated carbon granular, respectively. It can be seen from these Figures that the majority of pores on the surface of ACF and ACG mesopores, hence, are more effective in adsorbing MB [35,36]. It can also be observed from these Figures that the number of pores on the surface of the prepared ACF is higher than that of commercial ACG. Moreover, this observation is in agreement with the results from surface analysis.

FT-IR spectroscopy was used to identify the functional groups on the surface of ACF and ACG. The spectra obtained are shown in Fig. 4. For ACF, the broad band at $3,348.25 \text{ cm}^{-1}$ is attributed to the presence of the hydroxyl group. The band located at around $2,949.53 \text{ cm}^{-1}$ corresponds to C–H vibration stretching. While the absorption peak recorded at

Table 1
Characteristics of the activated carbons

Type of activated carbon	Activated carbon fiber	Commercial activated carbon
Specific surface area (m ² /g)	5,435	1,061
Total pore volume (cm ³ /g)	4.043	0.559
Micropore volume (cm ³ /g)	1.479	0.328
Mesopore volume (cm ³ /g)	2.564	0.231
Average pore diameter (Å)	29.76	21.06
Micropore %	36.582	58.68
Mesopore %	63.418	41.32
pH _{ZPC}	7.8	6.7

1,057.34 cm⁻¹ is attributed to the symmetrical angular deformation of ether [37]. Whereas for ACF, there are two absorption peaks at 3,434.43 and 1,633.36 cm⁻¹ which correspond to the hydroxyl group and axial deformation of carbonyl group (C=O), respectively.

3.2. Adsorption studies

3.2.1. Effect of initial adsorbate concentration on the adsorption process

The result on the effect of the initial concentrations of MB on its adsorption uptake at equilibrium was investigated and is presented in Fig. 5. This figure shows that the amount of MB adsorbed on both adsorbents increased with increasing initial concentrations from 10 to 600 mg/L. This means that an

increase in initial MB concentration resulted in increasing solute uptake. Similar observation has been reported earlier for various types of adsorbates and adsorbents (e.g. [30,38,39]). The rate of adsorption was greater for higher initial MB concentration because the initial MB concentrations provide an important driving force to overcome all mass transfer resistance of the dye between aqueous phase and solid phase. Hence, higher initial concentration of MB enhances adsorption process due to a higher interaction between the solute and the adsorbent. On the other hand, the amount adsorbed (q_e mg/g) is almost constant at initial concentrations of over 600 mg/L. This can be explained by the fact that all adsorption sites became saturated after 600 mg/L. Moreover, it can also be observed from Fig. 5 that the adsorption efficiency of ACF towards MB is higher than that of

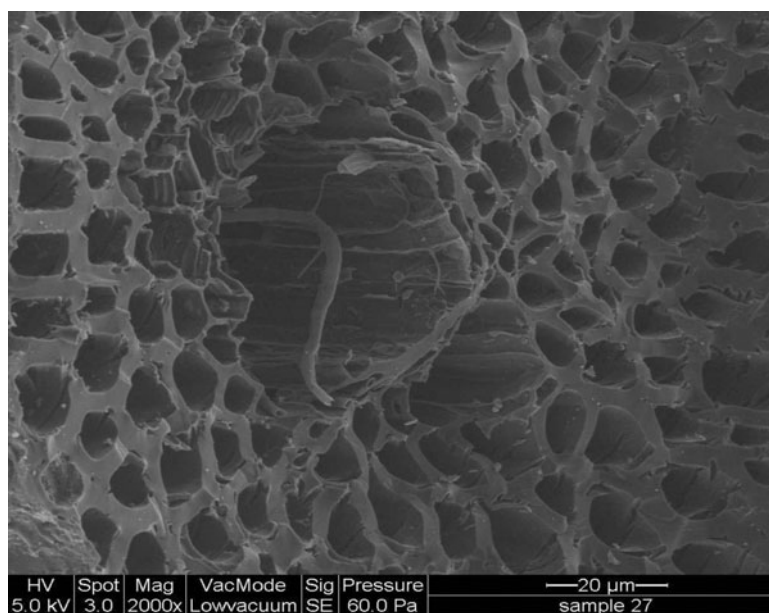


Fig. 2. SEM image of ACF.

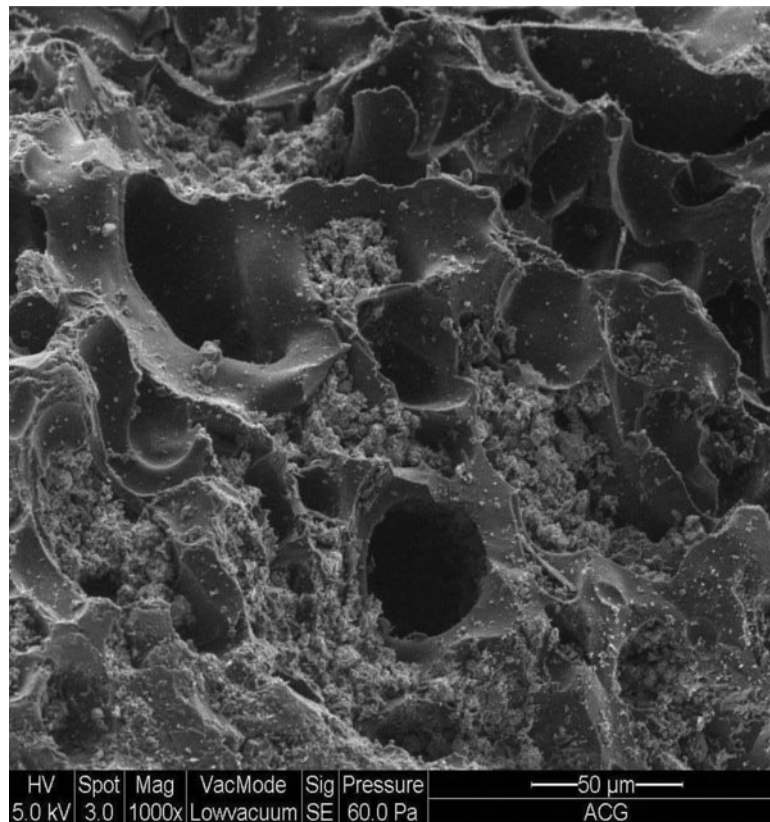


Fig. 3. SEM image of ACG.

ACG. This is because ACF has a higher surface area, larger pore diameter, higher total pore volume, higher mesopore volume, and larger mesopore percentage, which makes it more effective in adsorbing the dye. Similar observation was reported by Fernandes et al. [40].

3.2.2. Adsorption isotherms

The linear forms of the Langmuir (Eq. (1)) and the Freundlich (Eq. (2)) models were employed in this work in order to investigate the adsorption behavior.

$$\frac{C_e}{q_e} = \frac{1}{q_{\max} K_L} + \frac{C_e}{q_{\max}} \quad (1)$$

$$\ln q_e = \ln K_F + \frac{1}{n} \ln C_e \quad (2)$$

where q_e is the amount of the adsorbate adsorbed at equilibrium (mg/g), q_{\max} the maximum adsorption capacity corresponding to complete monolayer coverage on the surface (mg/g), and C_e is the concentration

of the adsorbate at equilibrium (mg/L). K_L is the Langmuir constant related to the energy or net enthalpy of adsorption. K_F is the Freundlich constant related to the adsorption capacity. $1/n$ is another constant in the Freundlich model related to the adsorption. If the value of $1/n$ is between 0 and 1, the adsorption is favorable [41].

The essential characteristics of the Langmuir isotherm can be expressed by a dimensionless factor called equilibrium parameter R_L which is defined by Eq. (3) [42].

$$R_L = \frac{1}{1 + K_L C_0} \quad (3)$$

where K_L is the Langmuir constant and C_0 is the initial adsorbate concentration. The value of R_L indicates the type of isotherm to be either unfavorable ($R_L > 1$), linear ($R_L = 1$), favorable ($0 < R_L < 1$), or irreversible ($R_L = 0$).

The plots of C_e/q_e vs. C_e and $\ln q_e$ against $\ln C_e$ are given in Figs. 6 and 7, respectively. The constants of Langmuir (q_{\max} and K_L) and Freundlich (K_F and n) isotherm models with the corresponding correlation

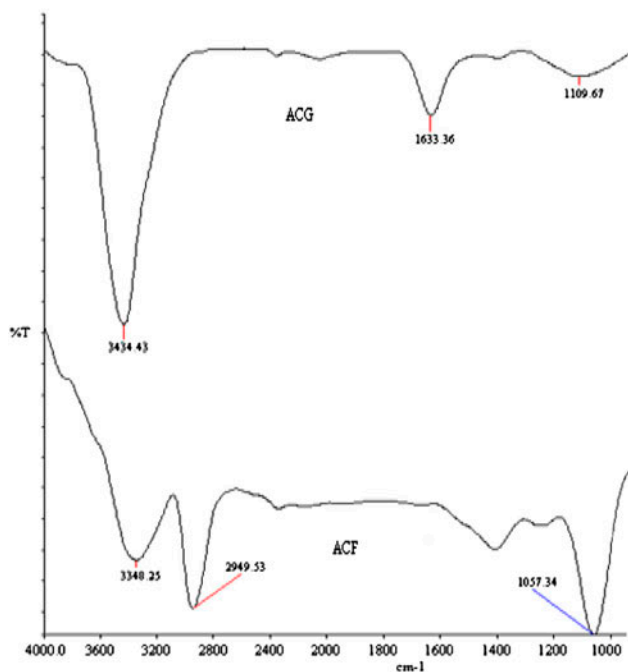


Fig. 4. FT-IR spectra for the prepared ACF and a commercial ACG.

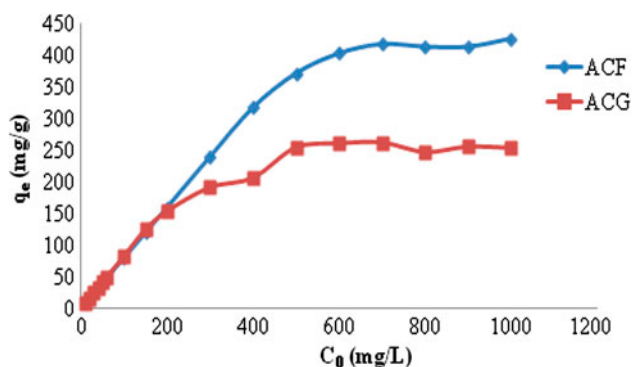


Fig. 5. Effect of initial concentration on the adsorption of MB on ACF and ACG.

coefficients (R^2) were calculated and their values listed in Table 2. The values of R_L were also calculated according to Eq. (3) and listed in Table 2. The values of R_L and $1/n$ (Table 2) were found to be between 0 and 1, indicating that both activated carbons (fibrous and granulated) adsorb MB favorably under the conditions studied. The correlation coefficients (R^2) for the Langmuir model are bigger than those of the Freundlich isotherm model, indicating that the former offers a better fit than the latter. This confirms that the surfaces of the activated carbons used in this work are uniform and the adsorption sites are of the same type.

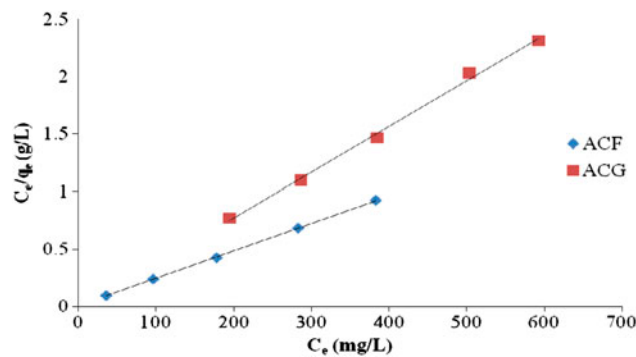


Fig. 6. Langmuir isotherm model for the adsorption of MB on ACF and ACG.

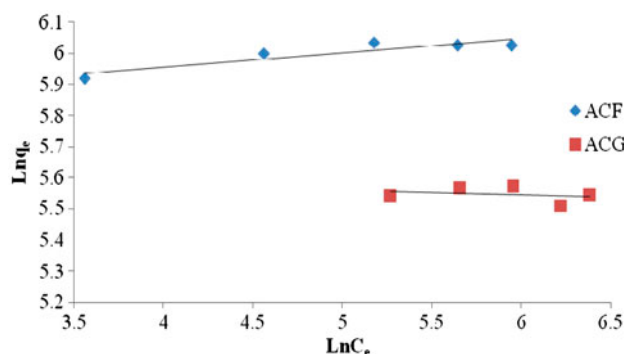


Fig. 7. Freundlich isotherm model for the adsorption of MB on ACF and ACG.

Similar results have been reported for the adsorption of MB on cedar sawdust and crushed brick [43].

It can also be seen from Table 2 that the values of q_{max} and K_F obtained for ACF are higher than those of ACG, which indicates that the former has better adsorption efficiency than the latter. This is due to the higher surface area and higher percentage of mesopores for ACF, hence, is more effective in adsorbing MB. Moreover, the number of pores in the surface of ACF is higher than that of ACG as shown in the Figs. 2 and 3.

3.2.3. Effect of agitation time

Figs. 8 and 9 show the adsorption uptake vs. the adsorption contact time at two initial MB concentrations (100 and 200 mg/L) for ACF and ACG, respectively. The amount of MB adsorbed increased with increasing agitation time and then reached a plateau. The equilibrium contact times in the case of ACF were 10 and 30 min for 100 and 200 mg/L concentrations, respectively. While, the adsorption of 100 and 200 mg/L solutions of MB on ACG reached the

Table 2
Langmuir and Freundlich parameters, and separation factors (R_L) for the adsorption of MB on ACF and ACG

Adsorbent	Langmuir isotherm				Freundlich isotherm			
	q_{\max} (mg/g)	K_L (L/mg)	R_L	R^2	K_F (mg/g) (L/mg) $^{1/n}$	$1/n$	n	R^2
ACF	500	0.286	0.0039	0.999	321.82	0.045	22.22	0.815
ACG	250	0.121	0.0091	0.996	278.11	0.013	76.92	0.069

equilibrium after 2 and 5 h, respectively. These results indicate that the adsorption of this dye on ACF is faster than that of on ACG. This, again, is because the former has a higher percentage (%) of mesopores and higher average pore diameter than that of the latter (Table 1). Similar results have been reported for the adsorption of MB on graphene [44].

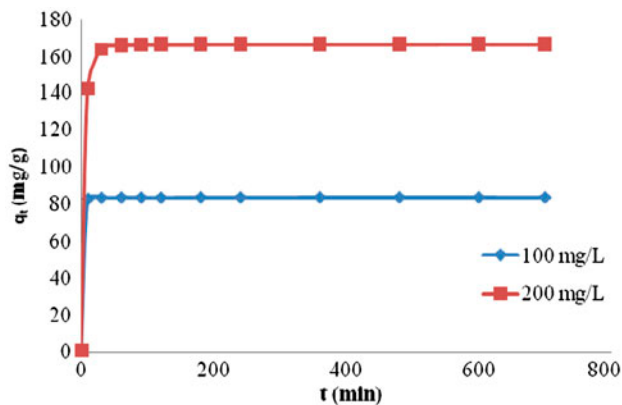


Fig. 8. The variation of the adsorption capacity of ACF with adsorption time at 100 and 200 mg/L concentrations of MB ($T=303$ K, $W=0.03$ g, and $V=25$ mL).

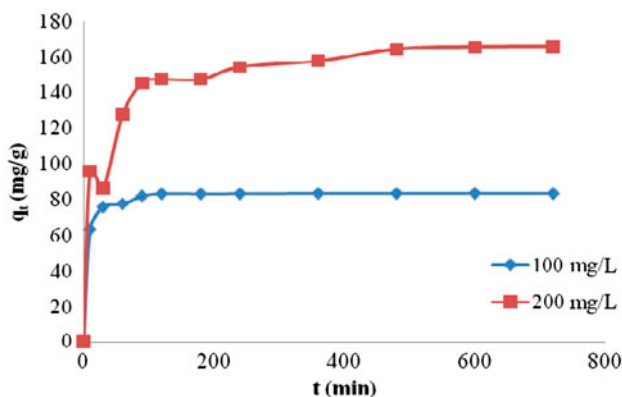


Fig. 9. The variation of the adsorption capacity of commercial activated carbon with adsorption time at 100 and 200 mg/L concentrations of MB ($T=303$ K, $W=0.03$ g, and $V=25$ mL).

3.2.4. Kinetic studies

In order to determine the mechanism of the adsorption of MB onto these adsorbents, the experimental data at two initial dye concentrations (100 and 200 mg/L) were analyzed by the pseudo-first-order, pseudo-second-order, and intra-particle diffusion kinetic models. The linearized-integral form of the pseudo-first-order model is expressed as follows:

$$\log(q_e - q_t) = \log q_e - K_1 \frac{t}{2.303} \quad (4)$$

where K_1 (min^{-1}) is the adsorption rate constant, and q_e and q_t are the amounts of dye adsorbed (mg/g) at equilibrium and time t (min). The values of K_1 and q_e were calculated from the slopes and intercepts of the plots of $\log(q_e - q_t)$ vs. t , which are presented in Figs. 10 and 11 for ACF and ACG, respectively. These values along with the correlation coefficients are listed in Table 3. It can be observed from Table 3 that the values of the correlation coefficients (R^2) are very small and the values of the calculated q_e are not in agreement with the experimental values of q_e for both adsorbents and at both concentrations. This indicates that the adsorptions of MB on ACF and ACG do not follow the pseudo-first order kinetic model. Similar results were observed by Tan et al. [10] and Liu et al. [44].

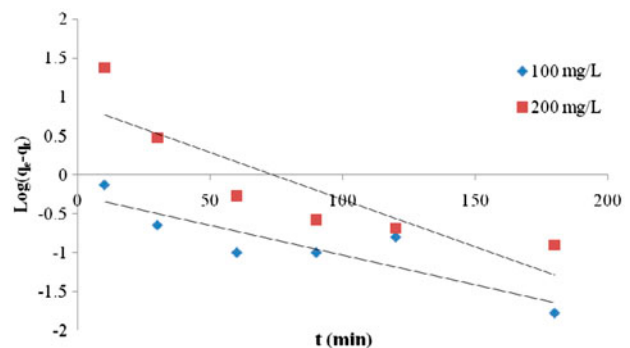


Fig. 10. Pseudo-first-order kinetics model for the adsorption of MB on ACF at 30 ± 1 °C.

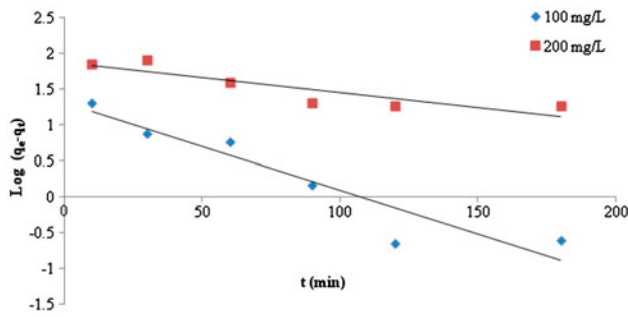


Fig. 11. Pseudo-first-order kinetics for the adsorption of MB on ACG at 30 ± 1 °C.

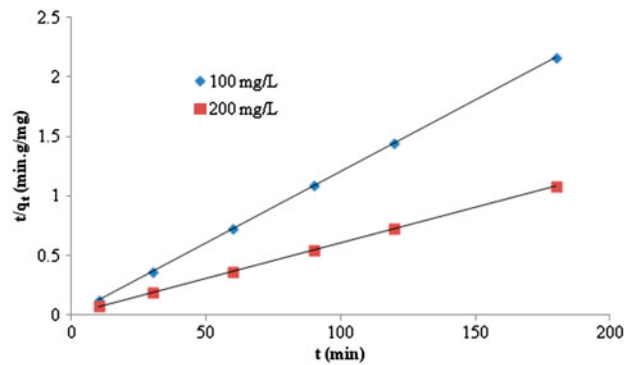


Fig. 12. Pseudo-second-order kinetics for the adsorption of MB on ACF at 30 ± 1 °C.

The linearized-integral form of the pseudo-second-order kinetic model is represented by Eq. (5):

$$\frac{t}{q_t} = \frac{1}{K_2 q_e^2} + \frac{t}{q_e} \quad (5)$$

where K_2 (g/mg min) is the rate constant of this model. The q_e and K_2 were calculated from the slopes and intercepts of the plots of t/q_t vs. t , which are demonstrated in Figs. 12 and 13 for ACF and ACG, respectively. The values of the pseudo-second-order kinetic model parameters are presented in Table 3. It can be seen from Table 3 that the values of R^2 are equal to one in the case of ACF, which is higher than that for the ACG (0.98). Moreover, it can be observed that there is a conformance between the experimental and the calculated q_e (Table 3) for both activated carbons. The results obtained here confirm the applicability of the pseudo-second-order kinetic model for describing the adsorptions of MB onto these adsorbents. The adsorption of MB on oil palm fiber-activated carbon [10] and grapheme [44] also follows pseudo-second-order kinetic model.

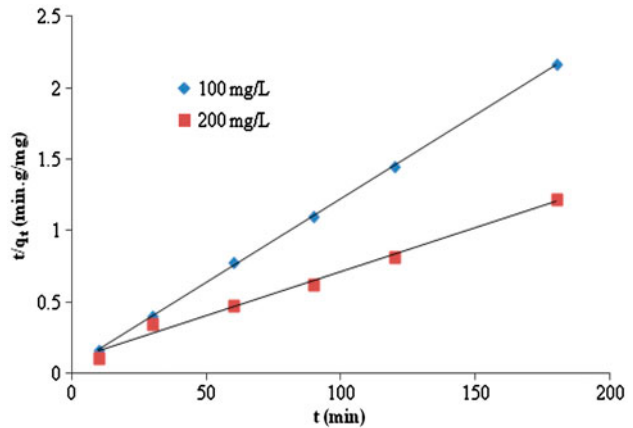


Fig. 13. Pseudo-second-order kinetics for the adsorption of MB on ACG at 30 ± 1 °C.

The linear form of the intra-particle diffusion (Eq. (6)) was used to determine the diffusion mechanism of the adsorption.

$$q_t = K_{dif} \sqrt{t} + C \quad (6)$$

Table 3

Comparison of pseudo-first-order and pseudo-second-order models for the adsorption of MB onto ACF and ACG at two initial dye concentrations and 30 ± 1 °C

Adsorbent	C_0 (mg/L)	$q_{e,exp}$ (mg/g)	Pseudo-first-order kinetics model			Pseudo-second-order kinetics model			
			$q_{e,cal}$ (mg/g)	K_1 (min^{-1})	R^2	$q_{e,cal}$ (mg/g)	K_2 (g/mg min)	R^2	Rate
ACF	100	83.17	1.85	0.016	0.786	83.33	0.144	1	12.00
	200	166.45	7.91	0.028	0.770	166.66	0.0060	1	0.999
ACG	100	83.20	20.23	0.028	0.884	90.91	0.0026	0.990	0.24
	200	165.87	73.79	0.009	0.788	166.66	0.0004	0.988	0.067

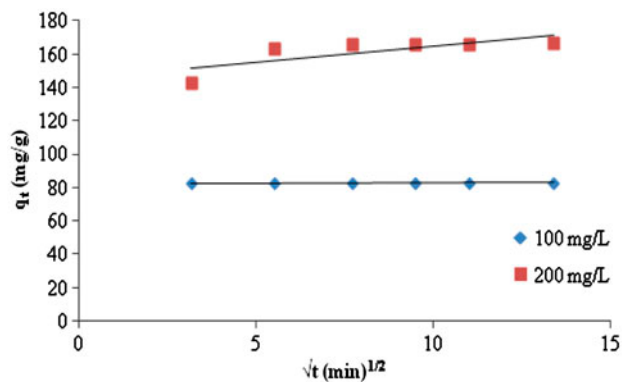


Fig. 14. Intra-particle diffusion model for the adsorption of MB onto ACF at $30 \pm 1^\circ\text{C}$.

where K_{dif} ($\text{mg/g min}^{1/2}$) is the rate constant of the intra-particle diffusion and C is the constant, which gives information about the thickness of the boundary layer [45].

The K_{dif} and C parameters were determined from the slopes and intercepts of the plots of q_t vs. $t^{1/2}$ (Figs. 14 and 15 for ACF and ACG, respectively). The values of the intra-particle diffusion parameters are summarized in Table 4. It can be clearly seen from Table 4 that the regression coefficient (R^2) values of the intra-particle diffusion are relatively small. The obtained results demonstrate that the intra-particle diffusion mechanism was not involved in the adsorption of MB by ACF and/or ACG. Altendor et al. [46] observed similar results in the case of MB and phenol adsorption onto activated carbon prepared from vetiver roots by chemical activation. In general, the results obtained in this work are in agreement with results reported in the literature for the adsorption of MB onto titanate nanotubes [47] and lotus leaf [48]. Furthermore, Table 3 illustrates that the adsorption

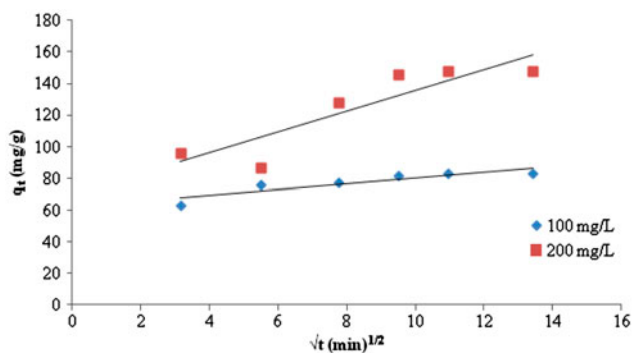


Fig. 15. Intra-particle diffusion model for the adsorption of MB onto ACG at $30 \pm 1^\circ\text{C}$.

Table 4

Parameter values of intra-particle diffusion model for the adsorption of MB on ACF and ACG at two initial dye concentrations and $30 \pm 1^\circ\text{C}$

Sample	C_0 (mg/L)	$q_{e,\text{exp}}$ (mg/g)	Intra-particle diffusion		
			K_{dif} ($\text{mg/g min}^{1/2}$)	C	R^2
ACF	100	83.17	0.057	82.46	0.657
	200	166.45	1.903	145.80	0.559
ACG	100	83.20	1.819	62.08	0.808
	200	165.87	6.603	69.79	0.796

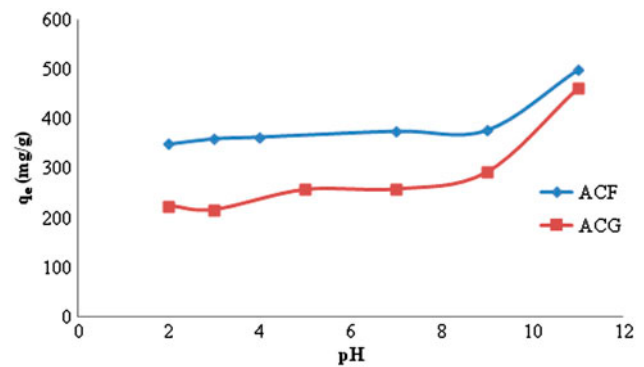


Fig. 16. Effect of initial pH on the adsorption of MB on ACF and ACG.

rates of this dye by ACF are higher than those of ACG. This is due the same reasons mentioned earlier in the study on the effect of adsorption time.

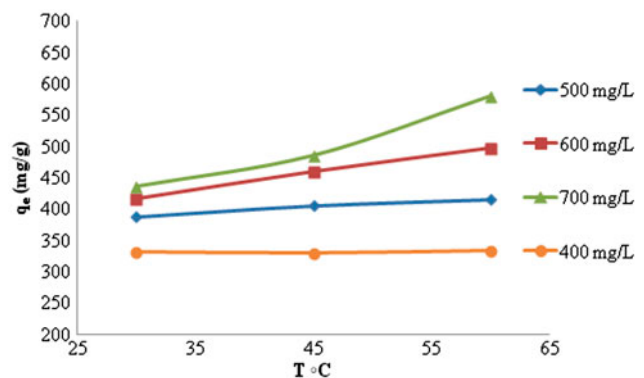


Fig. 17. Effect of temperature on the adsorption of MB on ACF at three different initial MB concentrations (400, 500, and 600 mg/L).

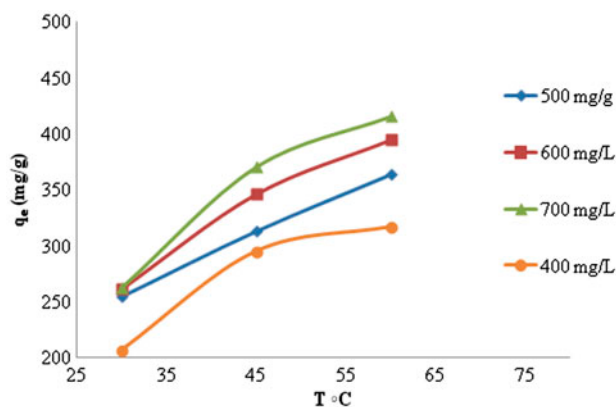


Fig. 18. Effect of temperature on the adsorption of MB onto ACG at three different initial MB concentrations (400, 500, and 600 mg/L).

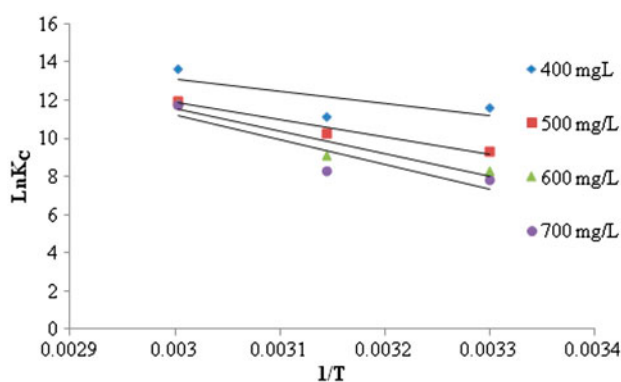


Fig. 19. Plots of $\ln K_c$ vs. $1/T$ for the adsorption of MB onto ACF at different dye concentrations.

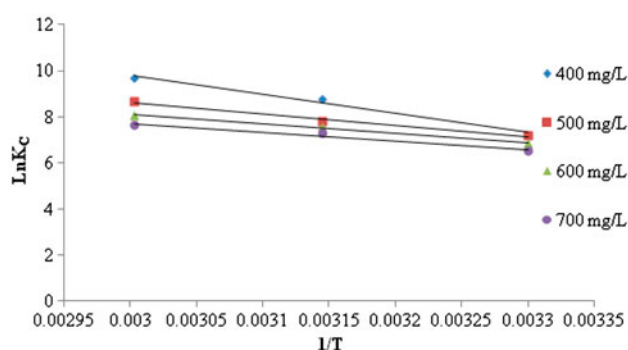


Fig. 20. Plots of $\ln K_c$ vs. $1/T$ for the adsorption of MB onto ACG at different dye concentrations.

3.2.5. Effect of pH on adsorption

The effect of pH on the adsorption of MB onto ACF and ACG is shown in Fig. 16. It is evident that the amounts of MB adsorbed at equilibrium show a slight increase as pH is increased within the range

under study. The pH_{ZPC} values for ACF and ACG were found to be 7.8 and 6.7, respectively. Upon dissolution, MB is ionized and thus releases positively charged ions into the solution [6]. The adsorption of these cations onto the adsorbent surface is primarily affected by the adsorbent surface charge, which is in turn affected by the solution pH [6]. The adsorbent surface charge is positive at $pH < pH_{ZPC}$ and negative when the solution $pH > pH_{ZPC}$. When the solution pH increased from the starting pH to pH_{ZPC} , the coulombic repulsions between the positively charged MB and the surface of the adsorbents are lowered. This explains the slight increase in the adsorption of this dye on both adsorbents. While, the sharp increase in the amounts of MB adsorbed onto these adsorbents at $pH > pH_{ZPC}$ carbons is due to the electrostatic attractions between the positively charged dye and the negative adsorbent surface. Similar trends were reported previously for the adsorption of MB onto jute fiber carbon [5]. It can also be observed from Fig. 15 that the maximum MB adsorptions onto both samples are at $pH = 11$, which is in agreement with the results reported in the literature for the adsorption of this dye on cotton stalk [6].

3.2.6. Effect of the temperature on adsorption

The effect of temperature on the adsorptions of MB onto ACF and ACG was examined at 30, 45, and 60 °C for three different initial dye concentrations (400, 500, and 600 mg/L). The results are represented in the Figs. 17 and 18 for ACF and ACG, respectively. These Figures demonstrate that the adsorption capacity of the two adsorbents increased with rising temperature of the solution, indicating that the processes are endothermic. This is due to the increase in the mobility of MB due to the increased in solution temperature [49]. An adequate energy may be also required for additional number of molecules to undergo an interaction with the active site at the surface [49]. Moreover, rising temperature may cause swelling for the internal structure of these adsorbents enabling extra number of the dye molecules to penetrate them [50]. Similar trends were reported in the literature for the adsorption of MB on garlic peel and agricultural waste biomass [49].

3.2.7. Adsorption thermodynamics

The thermodynamic parameters, including change in standard enthalpy (ΔH°), entropy (ΔS°), and free energy (ΔG°), were investigated using the following equations:

Table 5
Thermodynamic parameters of MB adsorption onto ACF and ACG ($T = 303, 318, \text{ and } 333 \text{ K}$)

Adsorbent	Initial concentration (mg/L)	ΔH° (kJ/mol)	ΔS° (kJ/mol)	ΔG° (kJ/mol)		
				303 K	318 K	333 K
Activated carbon Fiber (ACF)	400	54.48	0.273	-28.24	-32.33	-36.43
	500	74.80	0.323	-23.07	-27.91	-32.76
	600	97.65	0.389	-20.22	-26.05	-31.89
	700	109.17	0.421	-18.39	-24.71	-31.02
Activated carbon granular	400	69.20	0.290	-18.67	-23.02	-27.37
	500	41.28	0.196	-18.11	-21.05	-23.99
	600	34.67	0.171	-17.14	-19.71	-22.27
	700	31.19	0.158	-16.68	-19.05	-21.42

$$\text{Ln}K_C = -\frac{\Delta H^\circ}{RT} + \frac{\Delta S^\circ}{R} \quad (7)$$

$$K_C = \frac{q_e}{C_e} \times P$$

$$\Delta G^\circ = \Delta H^\circ - T \Delta S^\circ \quad (8)$$

where R is the universal gas constant (8.314 J/K mol), T is the adsorption temperature (K), and p is the density of the solution ($p = 1,000 \text{ g/L}$). The $\text{Ln}K_C$ was plotted against $1/T$ and shown in Figs. 19 and 20 for ACF and ACG, respectively. The values of ΔH° and ΔS° were computed from the slopes and intercepts of the above-mentioned plots. The values of ΔG° were calculated from the values of ΔH° and ΔS° using Eq. (10). The computed thermodynamic parameters are listed in Table 5. The positive values of ΔH° indicate that the adsorption of this dye on the ACF or ACG is endothermic in nature. This is in accordance with the results observed in the study on the effect of temperature earlier. The values of ΔH° (Table 5) are in the range of 54.48–109.17 and 31.19–69.20 for ACF and ACG, respectively. It was reported in the literature [9,34] that the adsorption enthalpy, ranging from 2.1 to 20.9 kJ/mol, corresponds to a physical adsorption. Therefore, the values of ΔH° obtained in this work suggest that the adsorption of MB on ACF and/or ACG can be classified as chemical adsorption. Moreover, it was found in the case of the adsorption kinetics that the experimental data described well by the pseudo-second-order model, indicating that the type of this adsorption is by chemisorption.

The positive ΔS° values suggest an increase in the randomness at the adsorbate solution interface during the adsorption process. The negative values of ΔG° suggest that the adsorption of MB onto any one of

these two adsorbent is spontaneous. It can also be observed from Table 5 that the values of ΔG° become more negative as the adsorption temperature increased for each concentration, indicating that higher temperature is the most favorable condition for the higher adsorption efficiency. Or in other words, the affinity of MB molecules to adsorb onto the surfaces of ACF and ACG increased with rising temperatures. The results obtained in this work are in agreement with the results reported previously for the adsorption of MB on kenaf core fibers [30], jatropha curcas [9], and neem leaf powder [51].

It can be seen from Table 5 that all of the thermodynamic parameters for the adsorption of MB onto the prepared ACF are higher than those of the commercial ACG, indicating that the adsorption affinity of the former towards MB is larger than that of the latter.

4. Conclusions

Coconut husk fiber was used as a starting material for the preparation of ACF. The physical and chemical properties of the prepared ACF and a commercially available ACG were investigated. The results obtained indicated that the adsorptive properties of ACF (For example: 5,435 m²/g surface area and 2.564 cm³/g mesopores volume) are better than those of ACG (1,061 m²/g surface area and 0.231 cm³/g mesopores volume). Langmuir and Freundlich models were applied to investigate the adsorption isotherms for the adsorption of MB, and it was found that the experimental data could be described well by the Langmuir model and the ACF has higher adsorption capacity (500 mg/g) than the ACG (250 mg/g). Adsorption kinetics was analyzed by pseudo-first-order, pseudo-second-order, and intra-particle diffusion kinetic models. The kinetic experimental data followed the pseudo-second-order model. It was observed the

adsorption rate of MB on ACF was higher than that for ACG. Thermodynamic parameters such as ΔH° , ΔS° , and ΔG° were calculated. The values of the parameters confirmed that the adsorption affinity of ACF towards MB is more significant than that of ACG. In general, the results obtained suggest that the ACF used in this work could be applied in wastewater treatment and superior than the commercial ACG.

Acknowledgments

This research was supported by the University of Malaya through a Postgraduate Research Grant PV035-2011A, for which the authors are very grateful.

References

- [1] A.M.M. Vargas, A.L. Cazetta, M.H. Kunita, T.L. Silva, V.C. Almeida, Adsorption of methylene blue on activated carbon produced from flamboyant pods (*Delonix regia*): Study of adsorption isotherms and kinetic models, *Chem. Eng. J.* 168 (2011) 722–730.
- [2] G. Christiansen, The toxicity of selected therapeutic agents used in cats, *Vet. Med. Small Anim. Clin.* 75 (1980) 1133–1137.
- [3] N.E. Camp, Methemoglobinemia, *J. Emerg. Nurs.* 33 (2007) 172–174.
- [4] S.S. Auerbach, D.W. Bristol, J.C. Peckham, G.S. Travlos, C.D. Hébert, R.S. Chhabra, Toxicity and carcinogenicity studies of methylene blue trihydrate in F344N rats and B6C3F1 mice, *Food Chem. Toxicol.* 48 (2010) 169–177.
- [5] S. Senthilkumar, P.R. Varadarajan, K. Porkodi, C.V. Subbhuraam, Adsorption of methylene blue onto jute fiber carbon: Kinetics and equilibrium studies, *J. Colloid Interface Sci.* 284 (2005) 78–82.
- [6] H. Deng, J. Lu, G. Li, G. Zhang, X. Wang, Adsorption of methylene blue on adsorbent materials produced from cotton stalk, *Chem. Eng. J.* 172 (2011) 326–334.
- [7] Y. Liu, Y. Zheng, A. Wang, Enhanced adsorption of methylene blue from aqueous solution by chitosan-g-poly (acrylic acid)/vermiculite hydrogel composites, *J. Environ. Sci.* 22(4) (2010) 486–493.
- [8] A. Mittal, V. Thakur, V. Gajbe, Adsorptive removal of toxic azo dye Amido Black 10B by hen feather, *Environ. Sci. Pollut.* 20 (2013) 260–269.
- [9] A. Kurniawan, S. Ismajli, Potential utilization of *Jatropha curcas* L. Press-cake residue as new precursor for activated carbon preparation: Application in methylene blue removal from aqueous solution, *J. Taiwan Inst. Chem. E.* 42 (2011) 826–836.
- [10] I.A.W. Tan, B.H. Hameed, A.L. Ahmad, Equilibrium and kinetic studies on basic dye adsorption by oil palm fiber activated carbon, *Chem. Eng. J.* 127 (2007) 111–119.
- [11] M.A.M. Salleh, D.K. Mahmoud, W.A.W. Abdul Karim, A. Idris, Cationic and anionic dye adsorption by agricultural solid wastes: A comprehensive review, *Desalination* 280 (2011) 1–13.
- [12] I.N. Najm, V.L. Snoeyink, B.W.J. Lykins, J.Q. Adams, Using powdered activated carbon: A critical review, *J. Am. Water Res.* 83 (1991) 65–76.
- [13] G.S. Prado Alexandre, D. Torres Jocilene, A. Faria Elaine, C.L. Dias Silvia, Comparative adsorption studies of indigo carmine dye on chitin and chitosan, *J. Colloid Interface Sci.* 277 (2004) 43–47.
- [14] S.J. Allen, B. Koumanova, Decolourisation of water/wastewater using adsorption (review), *J. Chem. Technol. Metall.* 40 (2005) 175–192.
- [15] V.C. Srivastava, I.D. Mall, I.M. Mishra, Characterization of mesoporous rice husk ash (RHA) and adsorption kinetics of metal ions from aqueous solution onto RH, *J. Hazard. Mater. B* 134 (2006) 257–267.
- [16] M. Hajjaji, A. Alami, A. El Bouadilii, Removal of methylene blue from aqueous solution by fibrous clay minerals, *J. Hazard. Mater. B* 135 (2006) 188–192.
- [17] A. Mittal, J. Mittal, L. Kurup, A.K. Singh, Process development for the removal and recovery of hazardous dye erythrosine from wastewater by waste materials–bottom ash and de-oiled soya as adsorbents, *J. Hazard. Mater. B* 138 (2006) 95–105.
- [18] A. Mittal, A. Malviya, D. Kaur, J. Mittal, L. Kurup, Studies on the adsorption kinetics and isotherms for the removal and recovery of methyl orange from wastewaters using waste materials, *J. Hazard. Mater.* 148 (2007) 229–240.
- [19] S. Wang, M. Soudi, L. Li, Z.H. Zhu, Coal ash conversion into effective adsorbents for removal of heavy metals and dyes from wastewater, *J. Hazard. Mater. B* 133 (2006) 243–251.
- [20] O. Hamdaoui, Dynamic sorption of methylene blue by cedar sawdust and crushed brick in fixed bed columns, *J. Hazard. Mater. B* 138 (2006) 293–303.
- [21] Z.U. Aksu, I.A. Isoglu, Use of agricultural waste sugar beet pulp for the removal of Gemazol turquoise blue-G reactive dye from aqueous solution, *J. Hazard. Mater. B* 137 (2006) 418–430.
- [22] E. Malkoc, Y. Nuhoglu, Removal of Ni(II) ions from aqueous solutions using waste of tea factory: Adsorption on a fixed-bed column, *J. Hazard. Mater. B* 135 (2006) 328–336.
- [23] A. Mittal, Adsorption kinetics of removal of a toxic dye, malachite green, from wastewater by using hen feathers, *J. Hazard. Mater. B* 133 (2006) 196–202.
- [24] V.K. Gupta, A. Mittal, L. Kurup, J. Mittal, Adsorption of hazardous dye, erythrosine, over hen feathers, *J. Colloid Interface Sci.* 304 (2006) 2–57.
- [25] V.K. Gupta, A. Mittal, Adsorptive removal of toxic azo dye Amido Black 10B by hen feather, *Toxicol. Environ. Chem.* 92 (10) (2010) 1813–1823.
- [26] A. Mittal, V. Thakur, V. Gajbe, Evaluation of adsorption characteristics of an anionic azo dye Brilliant Yellow onto hen feathers in aqueous solutions, *Environ. Sci. Pollut.* 19 (2012) 2438–2447.
- [27] V.K. Gupta, A. Mittal, D. Jhare, J. Mittal, Batch and bulk removal of hazardous colouring gent rose bengal by adsorption over bottom ash, *RSC Adv.* 2 (2012) 8381–8389.
- [28] A. Mittal, D. Jhare, J. Mittal, Adsorption of hazardous dye Eosin Yellow from aqueous solution onto waste material De-oiled Soya: Isotherm, kinetics and bulk removal, *J. Mol. Liq.* 179 (2013) 133–140.
- [29] S. Lei, J.-I. Miyamoto, H. Kanoh, Y. Nakahigashi, K. Kaneko, Enhancement of the methylene blue adsorption rate for ultramicroporous carbon fiber by addition of mesopores, *Carbon* 44 (2006) 1884–1890.
- [30] M.S. Sajab, C.H. Chia, S. Zakaria, S.M. Jani, M.K. Ayob, K.L. Chee, P.S. Khiew, W.S. Chiu, Citric acid modified kenaf core fibres for removal of methylene blue from aqueous solution, *Bioresour. Technol.* 102 (2011) 7237–7243.
- [31] I.A.W. Tan, A.L. Ahmad, B.H. Hameed, Adsorption of basic dye on high-surface-area activated carbon prepared from coconut husk: Equilibrium, kinetic and thermodynamic studies, *J. Hazard. Mater.* 154 (2008) 337–346.
- [32] Food and Agriculture Organization of the United Nations, Economic and Social Department, the Statistical Division, 2011, Available from: <http://faostat.fao.org/site/291/default.aspx>
- [33] K.Y. Foo, B.H. Hameed, Coconut husk derived activated carbon via microwave induced activation: Effects of activation agents, preparation parameters and adsorption performance, *Chem. Eng. J.* 184 (2012) 57–65.

- [34] S.K. Theydan, M.J. Ahmed, Adsorption of methylene blue onto biomass-based activated carbon by FeCl_3 activation: Equilibrium, kinetics, and thermodynamic studies, *J. Anal. Appl. Pyrolysis* 97 (2012) 116–122.
- [35] H. Tamai, M. Kouzu, H. Yasuda, Preparation of highly mesoporous and high surface area activated carbons from vinylidene chloride copolymer containing yttrium acetylacetonate, *Carbon* 41 (2002) 1645–1687.
- [36] J. Yamashita, T. Hirano, M. Shioya, Development of mesopores during activation of poly(vinylidene fluoride)-based carbon, *Carbon* 40 (2002) 1541–1548.
- [37] R.M. Silverstein, F.X. Webster, D.J. Kiemle, *Spectrometric Identification of Organic Compounds*, 7th ed., John Wiley & Sons, New York, 2005.
- [38] S. Karagöz, T. Tay, S. Ucar, M. Erdem, Activated carbons from waste biomass by sulfuric acid activation and their use on methylene blue adsorption, *Bioresour. Technol.* 99 (2008) 6214–6222.
- [39] J. Ma, Y. Jia, Y. Jing, Y. Yao, J. Sun, Kinetics and thermodynamics of methylene blue adsorption by cobalt-hectorite composite, *Dyes Pigm.* 93 (2012) 1441–1446.
- [40] A.N. Fernandes, C.A.P. Almeida, N.A. Debacher, M.M.D.S. Sierra, Isotherm and thermodynamic data of adsorption of methylene blue from aqueous solution onto peat, *J. Mol. Struct.* 982 (2010) 62–65.
- [41] G. Atun, G. Hisarli, W.S. Sheldrick, M. Muhlerler, Adsorptive removal of methylene blue from colored effluents on fuller, s earth, *J. Colloid Interface Sci.* 261 (2003) 32–39.
- [42] T.W. Weber, P. Chakkravorti, Pore and solid diffusion models for fixed-bed adsorbers, *Alchf J.* 20 (1974) 220–228.
- [43] O. Hamdaoui, Batch study of liquid-phase adsorption of methylene blue using cedar sawdust and crushed brick, *J. Hazard. Mater. B* 135 (2006) 264–273.
- [44] T. Liu, Y. Li, Q. Du, J. Sun, Y. Jiao, G. Yang, Z. Wang, Y. Xia, W. Zhang, K. Wang, H. Zhu, D. Wu, Adsorption of methylene blue from aqueous solution by graphene, *Colloid Surf. B* 90 (2012) 197–203.
- [45] F. Ahmad, W.M.A.W. Daud, M.A. Ahmad, R. Radzi, Using cocoa (*Theobroma cacao*) shell-based activated carbon to remove 4-nitrophenol from aqueous solution: Kinetics and equilibrium studies, *Chem. Eng. J.* 178 (2011) 461–467.
- [46] S. Altenor, B. Carene, E. Emmanuel, J. Lambert, J.-J. Ehrhardt, S. Gaspard, Adsorption studies of methylene blue and phenol onto vetiver roots activated carbon prepared by chemical activation, *J. Hazard. Mater.* 165 (2009) 1029–1039.
- [47] L. Xiong, Y. Yang, J. Mai, W. Sun, C. Zhang, D. Wei, Q. Chen, J. Ni, Adsorption behavior of methylene blue onto titanate nanotubes, *Chem. Eng. J.* 156 (2010) 313–320.
- [48] X. Han, W. Wang, X. Ma, Adsorption characteristics of methylene blue onto low cost biomass material lotus leaf, *Chem. Eng. J.* 171 (2011) 1–8.
- [49] B.H. Hameed, A.A. Ahmad, Batch adsorption of methylene blue from aqueous solution by garlic peel, an agricultural waste biomass, *J. Hazard. Mater.* 164 (2009) 870–875.
- [50] M. Alkan, M. Dogan, Adsorption kinetics of Victoria blue onto perlite, *Fresenius Environ Bull.* 12 (2003) 418–425.
- [51] Kr.G. Bhattacharyya, A. Sharma, Kinetics and thermodynamics of methylene blue adsorption on neem (*Azadirachta indica*) leaf powder, *Dyes Pigm.* 65 (2005) 51–59.